Single-frequency BDS/GPS RTK with low-cost U-blox receivers

Conference Paper · May 2017

DOI: 10.1109/CPGPS.2017.8075131

CITATIONS
16

READS
1,369

2 authors:

Tianxia Liu
The Hong Kong Polytechnic University
8 PUBLICATIONS **89** CITATIONS
SEE PROFILE

Bofeng Li
Tongji University
190 PUBLICATIONS **2,815** CITATIONS
SEE PROFILE

Single-frequency BDS/GPS RTK With Low-cost U-blox Receivers

Tianxia Liu, Bofeng Li
College of Surveying and GeoInformatics
Tongji University
Shanghai, China
E-mail: bofeng_li@tongji.edu.cn

***Abstract*—Technology of low-cost single-frequency RTK (real time kinematic) is booming in popular GNSS application, however, the poor data quality and hardware performance of low-cost receivers bring about great challenges to its positioning algorithm. In this contribution, a BDS/GPS single-frequency inexpensive navigation and positioning (SINAP) system is developed to achieve high-precise high-stability single-frequency RTK positioning with low-cost GNSS receivers. In data processing, we implement the kalman filter estimation with constant velocity (CV) and constant acceleration (CA) dynamic models. Since it is not feasible to fix the whole integer ambiguities in real applications, we utilize the PAR (partial ambiguity resolution) method to acquire a subset of integer ambiguities effectively. Experiments with static and kinematic data were carried out by using low-cost single-frequency u-blox receivers. To emphasize the benefits of the proposed method, we compare the performance of SINAP to those of the open source software RTKLIB and the u-blox chip. It is shown that results of SINAP are competitive to the ones of u-blox and outperform the ones of RTKLIB. Moreover, the performance of GPS-only, BDS-only and combination of BDS/GPS are investigated. The results reveal that using BDS/GPS can achieve higher fix-rate and higher positioning accuracy than using GPS or BDS only. Additionally, with kalman filter, we compare the CA and the CV dynamic models using kinematic data, which illustrates that both models can provide comparatively ideal results with no obvious difference.**

Keywords—single-frequency; low-cost; BDS/GPS; RTK;

I. INTRODUCTION

Thanks to the small size, low price and easy-embedding, the low-cost GNSS receivers have great application markets. They can easily be embedded into mobile phones, smart vehicles or other portable positioning advices to provide PNT service [1]. Moreover, low-cost RTK could also be applied in some traditional areas, such as geodetic monitoring, intelligent transport, precise farming and related location based service [2].Compared to the traditional survey-grade receivers, the low-cost receivers have obvious cost advantage. However, data of low-cost receivers usually have unsatisfactory quality owning to their poor hardware performance, for instance, frequent loss of lock, unpredictable data gap, less observations and low signal-to-noise ratio. Besides, most low-cost GNSS receivers only output single-frequency signals, which make it infeasible to eliminate the systematic errors and detect the cycle slips with combination of different frequencies. For low-cost GNSS receivers, above-mentioned limitations bring in great difficulties in high-precise positioning. Hence, the main challenge for low-cost RTK application is to study an advanced algorithm, which can achieve precise and stabile single-frequency RTK positioning solutions.

In recent decades, many studies have been done for RTK positioning with low-cost GNSS receivers [3-4]. In most of them, algorithm from RTKLIB software [5] has been integrated into micro-processor to achieve on-board positioning calculation. Although some existing researches show that centimeter-level positioning can be obtained by using RTKLIB algorithm, the solutions of RTKLIB are somewhat instable in practical applications. Even though some kinds of low-cost receivers can provide meter-level real-time positioning service at the same time, their price is relatively high.

It is proven that the utilization of multi-GNSS systems can compensate the lack of redundancy in single-frequency RTK [6-8]. Thus the BeiDou Navigation Satellite System (BDS), which has attained Asia–Pacific regional operational status and will achieve its global service in 2020, is employed together with GPS in this study. Existing researches demonstrate that the integrated GPS/BDS results in remarkably improved ambiguity resolution and positioning performance over single constellation. In addition, some contributions [e.g., 7] proved that single-frequency GPS/BDS can offer competitive positioning results to dual-frequency GPS, which demonstrates the potential of single-frequency RTK in practical applications.

In this paper, an integrate BDS/GPS single-frequency RTK software with novel algorithms is developed to achieve high accuracy RTK positioning by using low-cost GNSS receivers. RTK model and the related theories are specified at first. Then, the major functional modules and the flowchart of the software are elaborated. Afterwards, experiments with static and kinematic data were carried out by using single-frequency u-blox receivers. Results from RTKLIB software and u-blox module are involved as a comparison. Besides, we analyze the positioning results of BDS-only, GPS-only and combined BDS/GPS, as well as the constant velocity (CV) and constant acceleration (CA) dynamic model with kalman filter process in the experiments. Finally, summary and discussion are given.

A. Observation Models

In double-differenced (DD) mode between receivers and satellites, all errors associated to both receivers and satellites,

like receiver and satellite clock errors and initial phase biases, are totally eliminated. For short baselines, the residual DD tropospheric delays after corrections with standard tropospheric model and the ionospheric delays can be basically ignored. As a result, the single-frequency DD observation equations of code and phase read:

$$p_{br}^{ik} = \rho_{br}^{ik} + \varepsilon_{br}^{ik} \tag{1}$$

$$\phi_{br}^{ik} = \rho_{br}^{ik} + \lambda N_{br}^{ik} + \varepsilon_{br}^{ik} \tag{2}$$

where the subscript b and r represent the base and rover station, respectively. The subscript k and i represent two satellites.p and ϕ denote the code and phase measurements in meters. ρ stands for the receiver-to-satellite geometric distance. Nstands for the integer DD ambiguity with wavelength λ.ε_{br}^{ik} and ε_{br}^{ik} are the DD random noises of code and phase, respectively. The linearized single-epoch DD observation equations with respect to the coordinates read:

$$\boldsymbol{l}_p = \boldsymbol{A}\boldsymbol{x} + \boldsymbol{\varepsilon}_p, \;\; \boldsymbol{Q}_{\boldsymbol{\varepsilon}_p} \tag{3}$$

$$\boldsymbol{l}_\phi = \boldsymbol{A}\boldsymbol{x} + \lambda\boldsymbol{N} + \boldsymbol{\varepsilon}_\phi, \;\; \boldsymbol{Q}_{\boldsymbol{\varepsilon}_\phi} \tag{4}$$

where $\boldsymbol{l}_p$ and $\boldsymbol{l}_\phi$ are the observed-minus-computed observation vectors. $\boldsymbol{x}$ is coordinate unknowns with design matrix $\boldsymbol{A}$. $\boldsymbol{Q_p}$and$\boldsymbol{Q}_\phi$are the covariance matrices of single-epoch code and phase measurements, respectively. The single-epoch normal equations can be derived with least squares criterion as:

$$\begin{bmatrix} \boldsymbol{A^T}(\boldsymbol{Q_p^{-1}} + \boldsymbol{Q_\phi^{-1}})\boldsymbol{A} & \lambda\boldsymbol{A^T}\boldsymbol{Q_p^{-1}} \\ \lambda\boldsymbol{Q_p^{-1}}\boldsymbol{A} & \lambda^2\boldsymbol{Q_\phi^{-1}} \end{bmatrix} \begin{bmatrix} \widehat{\boldsymbol{x}} \\ \widehat{\boldsymbol{N}} \end{bmatrix} = \begin{bmatrix} \boldsymbol{A^T}\boldsymbol{Q_p^{-1}}\boldsymbol{l_p} \\ \boldsymbol{A^T}\boldsymbol{Q_\phi^{-1}}\boldsymbol{l_\phi} \end{bmatrix} \tag{5}$$

B. Stochastic Models

To specify the quality of observations at different elevations, an elevation-dependent weighting model is adopted to determine the variance of undifferenced observations as

$$\sigma^2 = (\frac{1.02}{\sin\theta + 0.02})^2 \sigma_0^{\,2} \tag{6}$$

where θ is the satellite elevation. Afterwards, the DD cofactor matrix$\boldsymbol{Q}_{DD}$ can be easily derived via the error propagation law. Since there is no common frequency of GPS and BDS, the reference satellite should be set separately for each system.

C. Kalman Filterestimation

The Kalman Filter(KF) is an efficient sequential estimation method widely applied in GNSS navigation[9-11]. The KF model consists of a set of dynamic equations and DD observation equations:

$$\boldsymbol{x}_k = \boldsymbol{\Phi}_{k-1,k}\boldsymbol{x}_{k-1} + \boldsymbol{w}_k, \;\; \boldsymbol{Q}_{\boldsymbol{w}_k} \tag{7}$$

$$\boldsymbol{l}_k = \boldsymbol{H}_k\boldsymbol{x}_k + \boldsymbol{\varepsilon}_k, \;\; \boldsymbol{Q}_{\boldsymbol{\varepsilon}_k} \tag{8}$$

where the subscript k represents the kth epoch. $\boldsymbol{x}$ denotes the state vector. $\boldsymbol{\Phi}_{k-1,k}$ denotes the state transition matrix that transfers the state vector from the $(k-1)$th epoch to the kth epoch. $\boldsymbol{w}_k \sim N(0, \boldsymbol{Q}_{\boldsymbol{w}_k})$ is the process noise in dynamic model, $\boldsymbol{\varepsilon}_k \sim N(0, \boldsymbol{Q}_{\boldsymbol{\varepsilon}_k})$ is the observation noise. Both of them are normal distribution with zero-mean and assumed to be non-correlated.$\boldsymbol{l}_k = [\boldsymbol{l}_p^{\mathrm{T}}\boldsymbol{l}_\phi^{\mathrm{T}}]^{\mathrm{T}}$, $\boldsymbol{H}_k$ is the design matrix.

According to the dynamic model, the predicted state $\tilde{\boldsymbol{x}}_k$ and its covariance $\boldsymbol{Q}_{\tilde{\boldsymbol{x}}_k}$can be obtained by using the solution of the former epoch:

$$\tilde{\boldsymbol{x}}_k = \boldsymbol{\Phi}_{k-1,k}\hat{\boldsymbol{x}}_{k-1} \tag{9}$$

$$\boldsymbol{Q}_{\tilde{\boldsymbol{x}}_k} = \boldsymbol{\Phi}_{\boldsymbol{k-1,k}}\boldsymbol{Q}_{\hat{\boldsymbol{x}}_{\boldsymbol{k-1}}}\boldsymbol{\Phi}_{\boldsymbol{k-1,k}}^{\boldsymbol{T}} + \boldsymbol{Q}_{\boldsymbol{w}_k} \tag{10}$$

Then the state vector of the current epoch can be solved:

$$\hat{\boldsymbol{x}}_k = \tilde{\boldsymbol{x}}_k + \boldsymbol{K}_k(\boldsymbol{l}_k - \boldsymbol{H}_k\tilde{\boldsymbol{x}}_k) \tag{11}$$

$$\boldsymbol{Q}_{\hat{\boldsymbol{x}}_k} = (\boldsymbol{I} - \boldsymbol{K}_k\boldsymbol{H}_k)\boldsymbol{Q}_{\tilde{\boldsymbol{x}}_k} \tag{12}$$

$$\boldsymbol{K_k} = \boldsymbol{Q}_{\tilde{\boldsymbol{x}}_k}\boldsymbol{H}_k^{\mathrm{T}}(\boldsymbol{H}_k\boldsymbol{Q}_{\tilde{\boldsymbol{x}}_k}\boldsymbol{H}_k^{\mathrm{T}} + \boldsymbol{Q}_{\boldsymbol{\varepsilon}_k})^{-\boldsymbol{1}} \tag{13}$$

The results of the current epoch also be used to predict the state parameters of next epoch.

As we all know, identifying a suitable dynamic model to describe the vehicle's dynamics is important. In this study, the commonly used dynamic model, the constant velocity(CV) model and the constant acceleration(CA) model are individually implemented. It is proved that both CV and CA models can achieve accurate RTK positioning in case of high sampling rates. The detailed information of two dynamic models is shown in Table Ⅰ. To ease the programming, the DD ambiguity parameters are meanwhile incorporated in KF, the state transition equation reads:

$$\boldsymbol{a}_k = \boldsymbol{a}_{k-1} + \boldsymbol{w}_a, \;\; \boldsymbol{Q}_{\boldsymbol{w}_k} = \sigma_{\boldsymbol{w}_a}^2\boldsymbol{I}_m \tag{14}$$

where $\boldsymbol{a}$ denotes the ambiguity unknowns, and its variance $\sigma_{\boldsymbol{w}_a}^2$can be assigned extremely small value, e.g.$\sigma_{\boldsymbol{w}_a}^2 = e^{-16}$, to characterize its constant property. If no integer ambiguity is fixed, the dimension of DD float ambiguity will be $n_s - 1$where$n_s$being the number of satellites. Notably, the number of parameters in the KF state vector will change once the float ambiguities are fixed or the available satellites vary in adjacent epochs.

TABLE I. STATE PARAMETERS IN KALMAN FILTER

states of KF	Dimension	Comments
Position(x, y, z)	3	Mandatory
Velocity (v_x, v_y, v_z)	3	Optional
Acceleration(a_x, a_y, a_z)	3	Optional
DDfloat ambiguity	Changeable	Optional

D. Partial Ambiguity Resolution

In real situation, the full ambiguities cannot be fixed simultaneously owning to their varying precisions. It is known that the precise of float ambiguity will improve along with the increased accumulation data in the filtering. With continuous observation in RTK data processing, new ambiguities are introduced from time to time which causes different accumulated time and varying precisions of different ambiguity unknowns. Moreover, the low-elevation satellites may suffer from relatively larger atmospheric errors as well as multipath effects, which results in different observation strength. All these factors bring in varying ambiguity precision and make it infeasible to fix the whole ambiguities simultaneously. As a result, the partial ambiguity resolution (PAR) method that allows fix a subset of the whole ambiguity parameters reliably is an efficient choice in real applications [12-15].

Let the float solution of $\hat{\boldsymbol{x}}_k$ and $\hat{\boldsymbol{a}}$ together with their covariance matrix obtained from KF as:

$$\begin{bmatrix}\hat{\boldsymbol{x}}_k\\ \hat{\boldsymbol{a}}\end{bmatrix},\ \begin{bmatrix}\boldsymbol{Q}_{\hat{\boldsymbol{x}}_k\hat{\boldsymbol{x}}_k} & \boldsymbol{Q}_{\hat{\boldsymbol{x}}_k\hat{\boldsymbol{a}}}\\ \boldsymbol{Q}_{\hat{\boldsymbol{a}}\hat{\boldsymbol{x}}_k} & \boldsymbol{Q}_{\hat{\boldsymbol{a}}\hat{\boldsymbol{a}}}\end{bmatrix} \tag{15}$$

In this study, the PAR method is employed and a subset of ambiguities is selected based on the accumulation time and the elevation of satellites. The procedure is as follows:

- Firstly, we select a subset of ambiguities that have been continuously tracked with a certain observation time span, for instance, 10 epochs, to guarantee the accumulated time of float ambiguities.
- Afterwards, we remove the ambiguities whose elevations are lower than an elevation threshold from the ambiguity subset, since the observations with lower elevations are more probably affected by the residual errors.
- Then, we apply the LAMBDA method [16]to efficiently solve out two optimal integer solutions in the subset and do ratio test. If the integer solutions pass the ratio test, we fix it and update the float solutions. If the ratio test is not passed, we iteratively increase the elevation threshold and repeat the steps 2 and 3. If it is finally not successful even with sufficient larger elevation threshold, the AR fails in this epoch.

Once the part of ambiguities$\hat{\boldsymbol{a}}_1$are successfully fixed, the equation(15) can be written into the following partitions:

$$\begin{bmatrix}\hat{\boldsymbol{x}}_k\\ \hat{\boldsymbol{a}}_1\\ \hat{\boldsymbol{a}}_2\end{bmatrix},\ \begin{bmatrix}\boldsymbol{Q}_{\hat{\boldsymbol{x}}_k\hat{\boldsymbol{x}}_k} & \boldsymbol{Q}_{\hat{\boldsymbol{x}}_k\hat{\boldsymbol{a}}_1} & \boldsymbol{Q}_{\hat{\boldsymbol{x}}_k\hat{\boldsymbol{a}}_2}\\ \boldsymbol{Q}_{\hat{\boldsymbol{a}}_1\hat{\boldsymbol{x}}_k} & \boldsymbol{Q}_{\hat{\boldsymbol{a}}_1\hat{\boldsymbol{a}}_1} & \boldsymbol{Q}_{\hat{\boldsymbol{a}}_1\hat{\boldsymbol{a}}_2}\\ \boldsymbol{Q}_{\hat{\boldsymbol{a}}_2\hat{\boldsymbol{x}}_k} & \boldsymbol{Q}_{\hat{\boldsymbol{a}}_2\hat{\boldsymbol{a}}_1} & \boldsymbol{Q}_{\hat{\boldsymbol{a}}_2\hat{\boldsymbol{a}}_2}\end{bmatrix} \tag{16}$$

here $\hat{\boldsymbol{a}}_2$ denotes the remaining float ambiguities. Then update the RTK solution with the partially fixed ambiguities:

$$\breve{\boldsymbol{x}}_k = \hat{\boldsymbol{x}}_k - \boldsymbol{Q}_{\hat{\boldsymbol{x}}_k\hat{\boldsymbol{a}}_1}\boldsymbol{Q}_{\hat{\boldsymbol{a}}_1\hat{\boldsymbol{a}}_1}^{-1}(\hat{\boldsymbol{a}}_1 - \breve{\boldsymbol{a}}_1) \tag{19}$$

$$\boldsymbol{Q}_{\breve{\boldsymbol{x}}_k\breve{\boldsymbol{x}}_k} = \boldsymbol{Q}_{\hat{\boldsymbol{x}}_k\hat{\boldsymbol{x}}_k} - \boldsymbol{Q}_{\hat{\boldsymbol{x}}_k\hat{\boldsymbol{a}}_1}\boldsymbol{Q}_{\hat{\boldsymbol{a}}_1\hat{\boldsymbol{a}}_1}^{-1}\boldsymbol{Q}_{\hat{\boldsymbol{a}}_1\hat{\boldsymbol{x}}_k} \tag{12}$$

Obviously $\boldsymbol{Q}_{\breve{\boldsymbol{x}}_k\breve{\boldsymbol{x}}_k} \le \boldsymbol{Q}_{\hat{\boldsymbol{x}}_k\hat{\boldsymbol{x}}_k}$, thus the precision of the RTK solution is improved.

Once the ambiguity is successfully fixed, the corresponding float parameters will be removed from the filtering state. The integer ambiguities will be delivered to the next epoch if no cycle slips occur, and the remaining float ambiguities are kept in the filter. With the data accumulation, they will be gradually fixed and the RTK solution will be continuously improved.

II. BDS/GPS SINGLE-FREQUENCY RTK IMPLENTMENTATION

Fig.1 illustrates the flowchart of RTK data processing in our software SINAP. The major functional modules including single point positioning (SPP), data preprocessing, cycle slips detection, KF estimation and partial ambiguity resolution are elaborated as follows:

- The SPP has been done by using BDS/GPS code observations to obtain some useful information, for instance, the satellite coordinates, clock bias and the initial coordinate of the rover station.
- The data preprocessing includes the cut-off elevation masking and the systematic error correction such as the relativistic correction, the earth rotation correction and the atmospheric delays correction. A predicted solution is firstly produced from KF to guarantee a continuous output in case the process cannot go on.
- DD code and phase observations are formed after preprocessing. The satellite with highest elevation is chosen as the reference satellite. Notably, if the reference satellite changes, the DD observations and DD ambiguities should be accordingly modified. Besides, the RTD solution is solved using DD code measurements.
- Cycle slips are detected and then repaired if cycle slips exist. Afterwards, the fixed ambiguities are delivered to the next epoch and the remaining float ambiguities are handled together with the positional, velocity and acceleration parameters in KF.
- After the KF updating, we acquire the final float solutions and its covariance matrix. Then the PAR and LAMBDA methods are employed to obtain the optimal integer ambiguities. Finally, the precise position is calculated with fixed ambiguities.

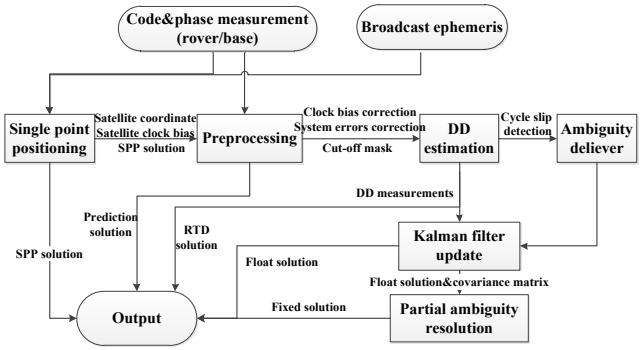

Fig. 1. Flowchart of BDS/GPS single-frequency RTKsystem

III. EXPERIMENTS AND ANALYSIS

A. Experiments Setup

Static and kinematic tests were carried out to evaluate the performance of the proposed algorithm. For rover and base stations, two single-frequency u-blox receivers are used to collect real GPS and BDS data with sampling interval of 1s. Both static and kinematic data are processed epoch by epoch in kinematic mode by SINAP. The elevation mask is set to 15° and the threshold of ratio testis set to 2. The data are processed by RTKLIB with the same ratio test threshold and with "Fix and Hold" AR strategy. Besides, results from u-blox chips are also involved in the experiment comparison.

B. Static test and analysis

A short baseline of 25.7 meters is chosen in the static test to valid the performance of the developed SINAP. Three datasets were collected on 14 September, 2016 and the dataset details are shown in Table II.

TABLE II. INFORMATION OF STATIC TEST DATASETS

	Start time	End time	# epochs
Data1	07:28:35	09:31:49	7358
Data2	09:33:06	11:19:30	6352
Data3	11:21:46	12:24:01	3663

Fig.2 shows the available satellites number and the PDOP value of three datasets using combined GPS/BDS. We can see that the available satellites are within 12to 16 except for the 2091th epoch in Data3 where only 8 BDS satellites are tracked. Most of the PDOP values are lower than 2 which denote stable satellite geometry. Integrated GPS/BDS RTK positioning results from SINAP, RTKLIB and u-blox of three datasets are depicted in Fig. 3-5, where blue and green represent the fixed and float solutions, respectively. Meanwhile, the corresponding statistical results (stander deviation and mean) are listed in Table III-V.

The percentage of fixed solution in Data1 is 99.63, 60.77 and 9.25% for SINAP RTKLIB and u-blox, respectively. From Fig.3, we can see that the results of SINAP are the most stable and precise one in Data1. In RTKLIB results, several meters offsets take place between 3388 and 3487 epoch, which are not shown in figure. After that the integer ambiguity cannot be fixed in about 30 min and its float results bias in decimeters. In u-blox results, it is observed that the fix-rate is relatively lower and the float results vary in one or two meters. Besides, sudden jumps also occur near the 3388 epoch of it. As a comparison, the results of SINAP have higher fix-rate and maintain positioning precision within several centimeter except a re-initialization.

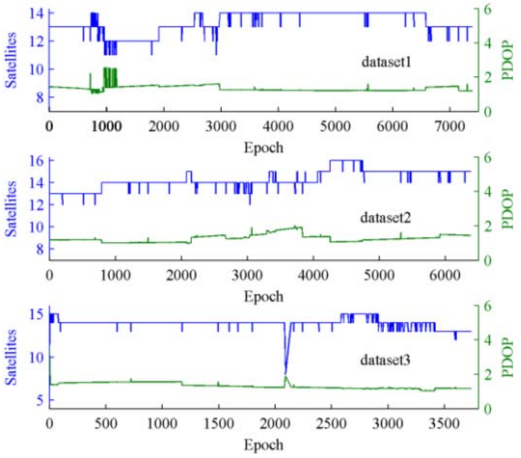

Fig. 2. Number of available satEellites and PDOP values of three datasets.

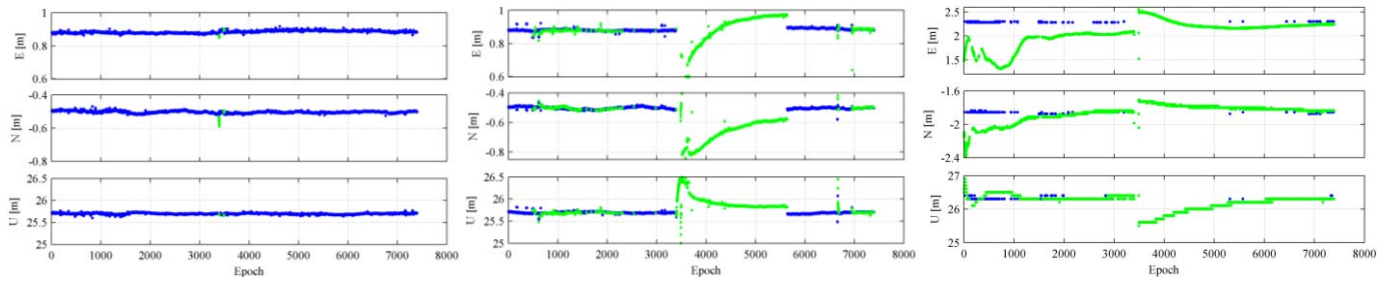

Fig. 3. SINAP (left), RTKLIB (middle) and u-blox (right)results of static data1 in N/E/U direction

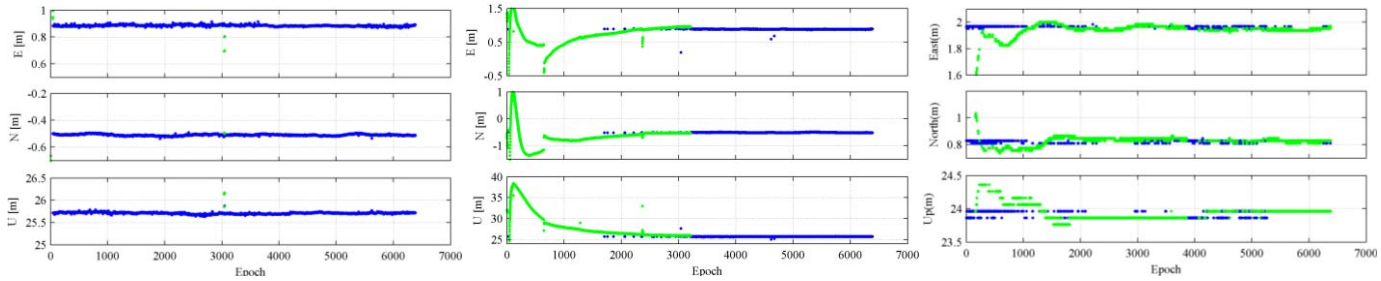

Fig. 4. SINAP (left), RTKLIB (middle) and u-blox (right)results of static data2 in N/E/U direction

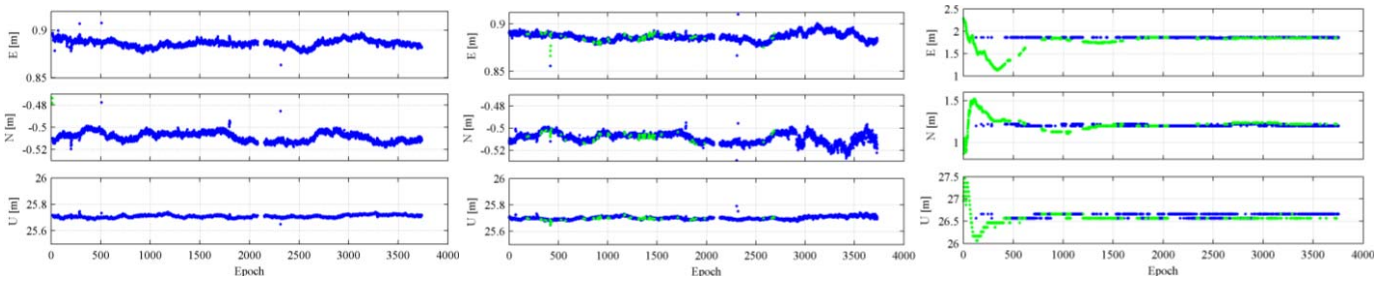

Fig. 5. SINAP (left), RTKLIB (middle) and u-blox (right)results of static data3 in N/E/U direction

TABLE III. STD AND MEAN OF FIXED SOLUTIONS FOR DATA1

	STD(mm)			MEAN(m)		
	E	**N**	**U**	**E**	**N**	**U**
SINAP	4.81	5.58	17.89	0.88	–0.51	25.70
RTKLIB	14.30	7.11	42.56	0.88	–0.51	25.71
u-blox	8.10	9.12	49.23	1.96	0.82	23.92

TABLE IV. STD AND MEAN OF FIXED SOLUTIONS FOR DATA2

	STD(mm)			MEAN(m)		
	E	**N**	**U**	**E**	**N**	**U**
SINAP	6.89	6.32	14.27	0.88	–0.50	25.70
RTKLIB	49.67	26.98	26.88	0.88	–0.50	25.69
u-blox	7.11	10.93	41.89	2.29	-1.86	26.33

TABLE V. STD AND MEAN FOR FIXED SOLUTIONS OF DATA3

	STD(mm)			MEAN(m)		
	E	**N**	**U**	**E**	**N**	**U**
SINAP	3.63	4.09	9.97	0.89	–0.51	25.71
RTKLIB	38.04	61.61	112.03	0.89	–0.51	25.70
u-blox	4.80	8.45	47.00	1.86	1.20	26.63

The proportion of fixed solution in Data2 is 99.2, 50.29 and 27.8% of SINAP, RTKLIB and u-blox, respectively. The time-to-first-fix of SINAP and RTKLIB are 10s and 53min, respectively. It is observed that, the results of SINAP have obvious advantage in fix-rate and fix-time. Besides, its STD values are smaller than the one of RTKLIB and u-blox. In contrast, it takes much longer time for RTKLIB to obtain stable fixed solutions and its STD values are up to centimeter-level. The results of u-blox are still barely fixed and the float solutions have fluctuation in several decimeters.

In Data3, the fix-rate is 99.4, 97.6 and 59.0% for SINAP, RTKLIB and u-blox, respectively. We can see that the fix-rate of RTKLIB and u-blox are apparently improved compared to the other two datasets. For u-blox results, the STD value of fixed solutions is within 1 cm in horizontal and 5 cm in vertical. And its float solutions have similar performance to Data1 and Data2. RTKLIB achieve high fix-rate in Data3 and the fixed solutions have same variation tendency in three coordinate directions of SINAP. Whereas, the STD value of the RTKLIB fixed solutions is much larger, which is up to nearly 10 times to the one of SINAP. That probably attributed to the increased dispersion in the last 1000 epochs and some sudden jumps.

TABLE VI. FIXING RATE OF STATIC DATASETS [%]

	SINAP			RTKLIB		
	GPS	**BDS**	**GPS/BDS**	**GPS**	**BDS**	**GPS/BDS**
Data1	0	0	99.6	0	0	60.8
Data2	0	99.0	99.2	0	34.9	50.2
Data3	0	63.2	99.4	0	99.3	97.6

Results shown above are all solved by integrated GPS/BDS systems. The experiments using each single system were carried out as well. The positioning results of GPS-only and BDS-only are not displayed due to the limited paper space, instead, the proportions of correctly fixed solutions of three datasets are shown in Table VI. For GPS-only, the correct-fix-rate is zero for all three datasets of both SINAP and RTKLIB. For BDS-only, the N/E/U STDs of dataset2 are (11.9, 8.6, 44.1mm) and (119.2, 51.8, 249.9 mm)for SINAP and RTKLIB, respectively. The N/E/U STDs of dataset3 are (42.2, 121.4, 1126.2 mm) and (39.4,78.3,162.7 mm) for SINAP and RTKLIB. It is obvious that the STDs of BDS-only are much larger than those of combined GPS/BDS solutions, see Tables III, IV and V. Hence, it is concluded that the utilization of combined GPS/BDS can further improve the correct-fix-rate and positioning accuracy compared with using single constellation.

C. Kinematic Test and Analysis

The kinematic test was carried out on 25 October 2016, from 08:44:02 to 09:34:04. The total number of epochs is 3003 and the area of the experiment place is over 200 m^2. First part of data is kinematic and the rest is static. Fig. 6 shows the number of available satellites and the associated PDOP values of GPS-only, BDS-only and combined GPS/BDS. We can see that the available satellites change more frequently than those in static test since more obstacles exist in kinematic situation. Moreover, the available satellites of BDS are larger than those of GPS, whereas PDOP values of GPS are smaller due to its well-geometry distribution. Additionally, the PDOP values of GPS/BDS are apparently smaller compared to GPS or BDS only, which reveals that the satellites geometry strength is further enhanced by the combination of BDS and GPS.

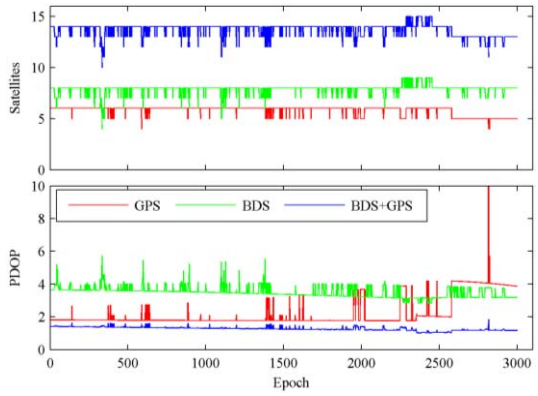

Fig. 6. Number of available satellites and PDOP values of kinematic data

The horizontal results using each of single system and combined BDS/GPS system are shown in Fig.7.In the static part of data, the ambiguities are not fixed in case of GPS/BDS. Meanwhile, they are wrongly fixed by single system with offsets in ±1 m. In the kinematic part of data, the proportion of fixed solutions is 19.7, 10.9 and 24.6%, and the corresponding time-to-first-fix is 268, 35 and 16 s for GPS-only, BDS-only and GPS/BDS, respectively. The results show that the fixing proportion and the fixing time are dramatically improved by using two systems together. As shown in Fig. 7, trajectories solved by each single system have some obvious bias in meters, which is vanished in BDS/GPS mode owning to the more redundancies and the less impact of systemic errors. For each single system, only 5-8 satellites are available shown in Fig. 6, which leads to the weak RTK model and hence worse positioning results. Considering the poor performance of the low-cost receivers, it is not feasible for single-frequency single-system RTK positioning in practice. Whereas, the combination of BDS and GPS overcomes the weakness of lack of the available satellites and provides more stable solutions.

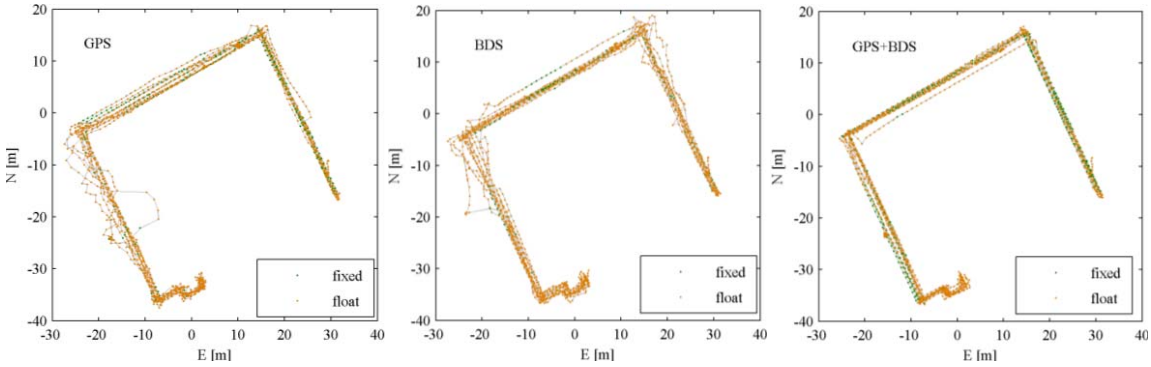

Fig. 7. Horizontal resultsof SINAP of GPS, BDS and BDS/GPS system from left to right

The trajectories of RTKLIB and u-blox using GPS/BDS are shown in Fig.8.Theirfix-rates are 17.0 and 55.0%, respectively. In RTKLIB results, some meter-level sudden jumps exist and its deviations are relatively large. In u-blox results, the trajectory is fairly smooth. Note that in both parts of kinematic and static, the u-blox results maintain the positioning errors within one to two meters without extreme large offset. The SINAP results with GPS/BDS performance much better than the one of RTKLIB and are competitive to the one of u-blox.

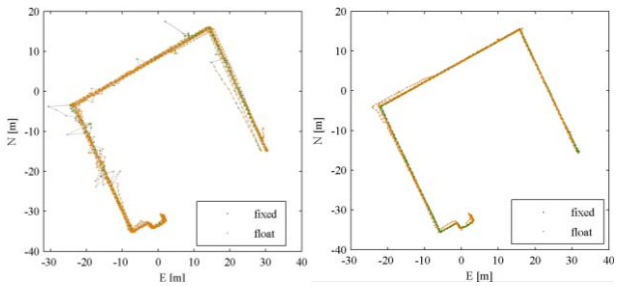

Fig. 8. Horizontal resultsof RTKLIB (left) and u-blox (right) of BDS/GPS system

It is known that the dynamic model in KF estimation impacts the positioning solutions as well. Since the SINAP solutions shown above are all using CV model, we display the results of CA model in this kinematic test. We show the horizontal results solved by CA model in Fig.9, the E/N/U results and the difference of CA and CV solutions in E/N/U directions in Fig.10. It is observed that the difference in static part is within±3 cm, but the one in kinematic part is within ±2 meters. Moreover, the peaks of the difference always appear at the peaks of the E/N/U solution where the variation of the velocity is relatively larger. In other words, the difference of CV and CA is not obvious in stable case, but it increases if the objects are under a complex motion state. Once the receiver follows a variable velocity motion that cannot be expressed by the CV model, the CA model is advised. That is why the CA model performs better than CV in the corn of the plane trajectory where the velocity of the receiver is changing. But using CA model also amplifies the value of offsets in the trajectory. All in all, using both CV and CA dynamic models can provide ideal RTK positioning results in this kinematic test.

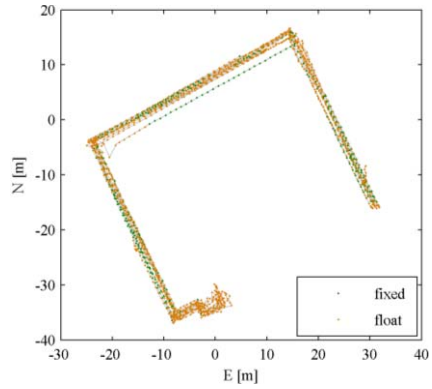

Fig. 9. Horizontal results of CA dynamic model

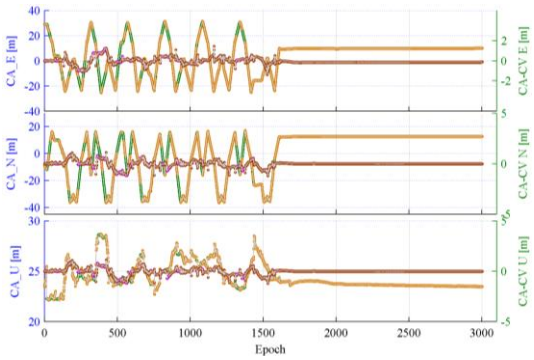

Fig. 10. Positioning results of CA dynamic model and the difference of CA and CV in E/N/U direction

IV. CONCLUSION

In this contribution, an integrated GPS/BDS RTK system is presented for low-cost single-frequency positioning. For data processing, the double-differenced observations are employed and the KF estimation with CV and CA dynamic models is implemented. The PAR with multiple criterions is adopted to reliably fix ambiguity subset. An independent developed single-frequency inexpensive navigation and positioning (SINAP) software is designed and its flowchart is elaborated.

The static and kinematic experiments with single-frequency u-blox receivers were conducted and the results were compared with those from RTKLIB software and u-blox module. In static tests, the proposed SINAP system can achieve centimeter-level solutions with higher ambiguity fix-rate and more stable positioning results by using GPS/BDS. In the kinematic test, the GPS/BDSSINAP results are relatively smooth and with no obvious offsets. The performance of SINAP is much better than that of RTKLIB and comparable to u-blox. Besides, the results of static and kinematic tests show that, the performance of combined GPS/BDS embodies a significant advantage in ambiguity fixing rate and positioning accuracy than that with GPS or BDS only. What's more, the CV and CA dynamic models are analyzed with kalman filter, and results show that both of them can provide desirable positioning results in kinematic test.

In general, the proposed algorithm in this paper can achieve relatively stable and precise RTK positioning results with GPS/BDS observations from low-cost single-frequency GNSS receivers.

ACKNOWLEDGMENTS

This work is supported by the National Natural Science Funds of China (41622401, 41574023, 41374031) and the National Key Research and Development Program of China (2016YFB0501802).

REFERENCES

[1] Luo B, Meng Q H, Xu F and JY Wang. Development of an on-board single-frequency GNSS RTK system for MAVs. Control Conference. IEEE, 2015:6005-6010.

[2] Caldera S, Realini E, Barzaghi R,M Reguzzoni and F Sansò. Experimental study on low-cost satellite-based geodetic monitoring over short baselines. J Surv Engi, 2016, 142(3):04015016.

[3] Stempfhuber W. 3D-RTK capability of single GNSSreceivers. ISPRS - International Archives of the Photogrammetry, Remote Sensing and Spatial Information Sciences, 2013.

[4] Takasu T, Yasuda A. Development of the low-cost RTK-GPS receiver with an open source program package RTKLIB. International Symposium on GPS/GNSS Jeju South Korea, 2009.

[5] RTKLIB, http://www.rtklib.com/, accessed 2017-04-10

[6] Odolinski R, Teunissen P J G, Odijk D. Combined BDS, Galileo, QZSS and GPS single-frequency RTK. GPS Solut, 2015, 19(1):151-163.

[7] Odolinski R, Teunissen P J G. Low-cost, high-precision, single-frequency GPS–BDS RTK positioning[J]. Gps Solutions, 2017:1-16.

[8] He H, Li J, Yang Y, et al. Performance assessment of single- and dual-frequency BeiDou/GPS single-epoch kinematic positioning. GPS Solut, 2014, 18(3):393-403.

[9] Brown, Robert Grover, and P. Y. C. Hwang.Introduction to random signals and applied Kalman filtering. John Wiley & Sons, 1997.

[10] Yang Y, He H, Xu G. Adaptively robust filtering for kinematic geodetic positioning. J. Geod, 2001, 75(2):109-116.

[11] Zhou Z, Li B. GNSS windowing navigation with adaptively constructed dynamic model. GPS Solut, 2015, 19(1):37-48.

[12] Teunissen P J G, Joosten P, Tiberius C C J M. Geometry-free Ambiguity Success Rates in Case of partial fixing. Proc of the National Technical Meeting of the Institute of Navigation, 1999:201-207.

[13] Li B, Shen Y, Feng Y, W Gao and L Yang. GNSS ambiguity resolution with controllable failure rate for long baseline network RTK. J Geod, 2014, 88(2):99-112.

[14] Li B, Feng Y, Gao W and Z Li. Real-time kinematic positioning over long baselines using triple-frequency BeiDou signals. IEEE Trans on Aerospace & Electronic Systems, 2015, 51(4):3254-3269.

[15] Odijk D. Predicting the Success Rate of Long-baseline GPS+Galileo (Partial) Ambiguity Resolution. J. Navigation, 2014, 67(3):385-401.

[16] Teunissen P J G. The least-squares ambiguity decorrelation adjustment: a method for fast GPS integer ambiguity estimation. J Geod, 1995, 70(1):65-82.